Advocating circular economy in wastewater treatment: Struvite formation and drinking water reclamation from real municipal effluents

Advocating circular economy in wastewater treatment: Struvite formation and drinking water reclamation from real municipal effluents

A. Mavhungu[1], V. Masindi[2,3&4*], S. Foteinis[5] R. Mbaya[1], M. Tekere[3], I. Kortidis[6], and E. Chatzisymeon[5]

[1]Department of Chemical, Metallurgy and Materials Engineering, Staatsartillirie Rd, Pretoria West 0183, Tshwane University of Technology, Pretoria, South Africa

[2]Council for Scientific and Industrial Research (CSIR), Built Environment (BE), Hydraulic Infrastructure Engineering (HIE), P.O Box 395, Pretoria, 0001, South Africa, Tel: +2712 841 4107, Fax: +27128414847, masindivhahangwele@gmail.com

[3]Department of Environmental Sciences, School of Agriculture and Environmental Sciences, University of South Africa (UNISA), P. O. Box 392, Florida, 1710, South Africa

[4]Magalies Water, Scientific Services, Research & Development Division, Erf 3475, Stoffberg street, Brits, 0250, tel: 0123816602

[5]School of Engineering, Institute for Infrastructure and Environment, University of Edinburgh, Edinburgh EH9 3JL, United Kingdom

[6]Department of Physics and Engineering, University of Zululand, Kwadlangezwa, 3886, South Africa

*Corresponding author: masindivhahangwele@gmail.com

Abstract

In this pilot study, the circular economy concept in wastewater treatment was examined, through a zero liquid discharge (ZLD) process where struvite was recovered and drinking water was reclaimed. A stage wise approach was used for struvite formation and the subsequent reclamation of drinking water. Specifically, the early stages of treatment entail the synthesis of struvite via the chemical precipitation of nutrients (phosphate and ammonia), using thermally activated cryptocrystalline magnesite. Thence, reverse osmosis (RO) was employed for drinking water reclamation. With this dual approach, 3.5 m^3 of municipal wastewater were successfully treated at a pilot plant in South Africa, producing ~52.5 kg of struvite and ~3.4 m^3 of drinking water. The operating parameters were 30 min of residence time, 0.5 g : 500 mL solid to liquid (S/L) ratio, using ambient temperature and pH. X-ray diffraction (XRD) and High Resolution Scanning Electron Microscopy (HR-SEM) coupled with electron dispersion spectroscopy (EDS) confirmed the synthesis of struvite and the presence of notable Mg/P ratios. Fourier Transform Infrared Spectrometer (FTIR) further ascertained the obtained results. Moreover, it was identified that the reclaimed water meets the South African National Standard (SANS) 241 and the world health organisation (WHO) standards for drinking water. An economic analysis revealed the viability of the process, suggesting that the system could be self-sustainable. Therefore, the results of this work indicate that introducing the concept of circular economy in wastewater treatment can promote the sustainable management of the ever-increasing quantities of municipal wastewater and at the same time address problems of emerging concern, such as water scarcity and phosphate shortage.

Keywords: Municipal wastewater; struvite synthesis; reclamation of drinking water; reverse osmosis (RO); circular economy

1 Introduction

Municipal wastewater influents and poorly treated effluents comprise a heterogeneous mixture of microbial, organic, and inorganic contents [1-5]. Of prime concern is the ubiquitous presence of ammonia, nitrate, and phosphate, which can pose a major environmental threat to the receiving ecosystem if not managed properly. In particular, nutrient enrichment can render the environment conducive to aquatic plant a rapid growth. However, when aquatic plants die, they deplete the dissolved oxygen in the water through aerobic decomposition. This create anoxic conditions, thus depriving aquatic organisms of oxygen. A vicious cycle begins, where the death of more aquatic organisms will ensue, which reduces the aquatic biodiversity and its ability to foster life, including benthic organisms and habitat [6-10]. In light of that, techno-viable wastewater management techniques need to be developed and implemented, particularly in low- and middle-income countries (LMIC) such as South Africa, to address this problem. According to various standards and water quality limits, the proposed level for ammonia and phosphate should be $\leq$1.5 mg L^{-1} and $\leq$10 mg L^{-1}, respectively, when discharged to the receiving environment, albeit ammonia can be converted into nitrate or nitrite with prescribed limits of $\leq$11 and $\leq$0.90 mg L^{-1}, respectively [11-14].

Nonetheless, the presence of ammonia and phosphate in municipal influents can also render them a viable option for their recovery through the synthesis of struvite [15-18]. In addition, the treated water can be further purified and reclaimed to address the alarming rate of water crisis, in South Africa and further afield. Specifically, according to the United Nations (UN) sustainable development report, by 2030 the water crisis will be very high in developing countries, primarily due to overpopulation and pollution [19].

This pilot study examines the performance of an actual struvite recovery system, scaled up at village-level and operating under the South African setting. Noteworthy, previous works focused on optimization of the operational parameters [1, 20], which were used for the sustainable and effective operation of this pilot unit. Furthermore, it was identified that ammonia removal was dependent on phosphate and magnesium concentration, with decreasing phosphate concertation largely affecting the system's efficacy in terms of ammonia removal [1].In light of that, a fixed system under optimised conditions, which will yield high efficacy for ammonia removal, was examined as will be demonstrated. In addition to struvite, drinking water was also recovered by means of reverse osmosis (RO) filtration. Specifically, in recent decades, RO has emerged as a promising technique for pollution abatement and drinking water production. This is owed to its excellent separation process, which exhibits a high rejection rate of water contaminants, including a broad range of organic and inorganic pollutants as well as micropollutants and microorganisms and pathogens [21-23]. When RO is used for municipal wastewater reclamation, it has been observed that Ca and Mg in wastewater can lead to membrane scaling, thus and antiscalant should be injected [24]. Several studies have used lime, lime/soda ash, $Al_2(SO_4)_3$, and Na_2CO_3, among others, to protect the membrane from fouling, scaling and metal poisoning [21, 23]. However, in this work MgO is used towards struvite formation, which suggest that through Mg scavenging from the wastewater its concentration can be minimized, thus largely avoiding the need for antiscalants.

Overall, in this industrially orientated study, a problematic liquid waste (municipal wastewater) is valorised in the context of circular economy and through a zero liquid discharge (ZLD) processes to synthesize struvite and reclaim drinking water. Furthermore,

87 struvite can be used as slow release fertiliser [25, 26] or for the production of phosphoric acid
88 [27-29], among others. This means that virgin materials that would consumed for the
89 manufacturing of these products are protected, while struvite can also address, at least partly,
90 the problem of the dwindling reserves of phosphate rock. In addition, the RO reclaimed
91 drinking water can also address water scarcity concerns, in South Africa and further afield.
92 Future works of our group will also focus on cost effective alternatives to RO filtration, such
93 as nanofiltration (NF) and ultrafiltration (UF) as well as on photocatalysis, given the high
94 number of annual sunshine hours in South Africa. Overall, the system is versatile, amenable
95 and retrofittable, hence denoting that it can be directly installed in different South African
96 set-ups and can be further scaled up to industrial systems. Finally, by being a ZLD processes
97 the environmental impacts from discharging poorly treated or untreated wastewater, a
98 problem in South Africa and other LMICs that are currently struggling to manage the ever-
99 increasing wastewater volumes due to rapid population growth, is also addressed. Therefore,
100 this is one of the first few study in design and execution of a closed loop system for
101 valorisation and beneficiation of real municipal influents in the circular economy context.

102 ## 2 Materials and methods

103 ### 2.1 System description

104 The stage wise treatment process, starting from raw municipal wastewater to struvite
105 recovery and drinking water reclamation, is shown in **Figure 1**. This process was
106 implemented at a pilot system, constructed at the premises of the Council for Scientific and
107 Industrial Research (CSIR) in Pretoria, with a treatment capacity of 3.5 m^3 per run (around
108 one hour).The pilot plant was found to be able to effectively treat raw municipal wastewater,
109 collected from a typical treatment plant in Pretoria. It should be noted that after collection,

110 the raw wastewater was simply screened before being fed into the pilot unit. Furthermore,
111 struvite was recovered and water that meets the South African National Standard (SANS)
112 241-2:2015 and the world health organisation (WHO) standards for drinking water was
113 reclaimed. The treatment process consists of five discrete stages, shown in **Figure 1**, while
114 their functions are described in **Table 1**.

115 ***Figure 1 here***

116 As shown in **Figure 1**, raw municipal influent is first introduced into a 3.5 m^3 clarifier, where
117 an overhead stirrer is in place. Then, the treatment process is carried out in five (5) stages,
118 which are: (1) struvite synthesis, (2) storage of the treated effluent, (3) treated effluent
119 purification by means of RO, (4) purified water storage, and finally (5) struvite storage. It
120 should be noted that the produced retentate is send back to the feed stream, i.e. to the raw
121 municipal effluent stream, while the filtrate from the filter press is send to the storage tank
122 (**Figure 1**). A discussion on the treatment process is given below.

123 ***Table 1 here***

124 **2.2 Synthesis of struvite**

125 The first stage of the treatment process is the synthesis of struvite by means of thermally
126 activated cryptocrystalline magnesite (calcined magnesite thereafter). The raw
127 cryptocrystalline magnesite activation process, along with the main characteristics of the
128 activated cryptocrystalline magnesite can be found in [1]. The conditions that optimize
129 struvite synthesis, both in terms of pollutants removal and environmental sustainability, were
130 adopted using the results of previous works of our group [1, 20]. Specifically, struvite was
131 synthesized at 30 minutes of equilibration time, using a 0.5 g calcined magnesite to 500 mL

wastewater ratio (i.e. 1 g L^{-1}), at ambient wastewater temperature and pH. After struvite formation, the treated effluent was left to settle for another 30 min and then the supernatant was moved to the holding tank (**Stage 2**). The produced sludge, which contains struvite, was dewatered using a filter press (**Stage 5**) and the filtrate was then directed a holding tank, where the supernatant is stored (**Figure 1**). The dewatered struvite was stored in a drying bed. The physicochemical and microbial parameters of the raw wastewater, the treated effluent, the reclaimed drinking water, and the recovered struvite were determined using state-of-the-art analytical techniques and are discussed below.

2.3 Drinking water reclamation

Drinking water was reclaimed by diverting the treated effluent from the holding tank to a RO unit for further polishing. Before the RO treatment, the calcined magnesite treated effluent was disinfected using chlorine, to remove biological contaminants such as microbes and *E.coli* and other coliform bacteria.

For RO membrane protection, the effluent was also dosed with 0.5 L diluted HCl (0.01M), to correct the pH to ~7.5, and 5 L of antiscalant solution (2 ppm concertation) per run (3.5 m^3 supernatant). The treated effluent was then diverted to the RO system for further purification (**Stage 3**). After treatment, drinking water was reclaimed and retentate was also produced. The drinking water was further purified by chlorination and moved to the purified water tank (**Stage 4**). The residual limit was maintained at <5 mgL^{-1} to ensure that the water remains disinfected throughout the supply chain until the end-user (Table 2). This was also conforming to the SANS 241-2:2015 and the WHO specifications for drinking water. The retentate was then diverted to the raw municipal wastewater stream for treatment (**Stage 1**).

2.4 Materials and chemical reagents

The raw municipal wastewater was collected from a treatment plant situated in Gauteng Province, South Africa, by means of a 10 m^3 vacuum truck. As such, seasonal variations in the chemical components of municipal wastewater were not considered. The source of magnesium oxide (MgO), which is required for nutrients precipitation from the wastewater, was prepared using raw cryptocrystalline magnesite, which was mined from an abandoned magnesite mine in Folovhodwe, South Africa. The raw magnesite was milled, then calcined at 1000 ℃, as to activate it, and then re-milled to fine powder [1]. Finally, commercially available and off-the-shelf chemicals, i.e. chlorine, HCl, and antiscalant, were used in the pilot system.

2.5 Reverse osmosis properties: membrane specifications and operating limits

In this study, a FilmTec™ BW30-4040 membrane was used, which is typically employed in light industrial applications, including for wastewater treatment [30]. The selected membrane is able to provide a reliable output of high quality water, which is required in order for the reclaimed water to meet SANS 241-2:2015 and the WHO specifications for drinking water. The properties and specifications of the reverse osmosis (RO) system are shown in **Table 2**.

Table 2 here

2.6 Characterisation

2.6.1 Aqueous characterisation

In-situ analyses for pH, electrical conductivity (EC), and total dissolved solids (TDS) were carried out using a multi-parameter probe (HANNA instrument, HI9828). Ex-situ analyses

were carried out in a South African National Standard (SANAS) accredited laboratory, located at CSIR, Pretoria, South Africa.

2.6.2 Solids characterisation

The analytical pieces of equipment that were used to identify the elemental composition, the morphological and chemical properties, and the metal functional groups of the raw andcalcined magnesite, as well as of the synthesized struvite are shown in **Table 3**. It should be noted that both the high-resolution scanning electron microscope (HR - SEM) and the high-resolution transmission electron microscope (HR - TEM) used in this work were coupled with an energy dispersive X-Ray spectroscopy (EDS) system.

Table 3 here

2.7 Economic analysis

A preliminary economic analysis of the assembled pilot plant was carried out to shed light on the estimated cost of the proposed technology and to quantify the possible economic gains of the recovered process co-products (struvite and drinking water). Specifically, both co-products have a commercial value, which only for the case of struvite can be as high as 200 USD (or R3 500) per ton, as is suggested in different chemical supply industries catalogues. Furthermore, in South Africa, there is no rural-urban tariff for potable water, since the cost is determined by consumption, with penalties in place for heavy consumers. Municipalities purchase water, in bulk supply, from commercial companies and typically sell it to end-users at a higher rate. In the context of this pilot study, a mean cost of 0.54 USD (or R9.10) per m^3 of drinking water was considered. Here, the economic analysis was focused on the direct field cost (DFC) and operational expenditure (OPEX), taking into account the following assumptions and limitations:

- The plant will operate 24 hours, 7 days a week (24/7), 360 days per year (to account for maintenance activities) with a minimal of 95% availability on an annual basis.
- Extraordinary conditions, such as flooding and climate extremes, which could hamper the plant's operation, are not included in the analysis.
- The supply and transportation cost of the municipal influent is deemed negligible as conventional treatment plants could be retrofitted with the proposed technology.
- In the economic analysis only the DFC and OPEX were considered, and thus labor costs and other possible expenditures are outside of this analysis.
- The electricity input required for the machinery operation is included in the analysis.

3 Results and discussion

3.1 Chemical characteristics of the raw wastewater and treated effluent

Table 4 list the chemical composition of the raw wastewater and of the effluent of each treatment stage, i.e. calcined magnesite treated effluent and RO water output. A discussion on the chemical characteristics of the effluent of each main stage of this technology, including the reclaimed drinking water is given below.

Table 4 here

3.1.1 Raw wastewater influent

As expected, the raw wastewater is rich in organic, inorganic, and biological contaminants and particularly in ammonia, phosphate, organic carbon, and bacteria content (**Table 4**). This can be attributed to decomposition of organic waste, which lead to the release of pathogenic bacteria, ammonia, and phosphate, among others. Specifically, *E. coli*, total coliform, and the

colony counts of the heterotrophic bacteria (i.e. total plate count) were very high, as was expected. This is also the case for ammonia, phosphate, colour, turbidity and conductivity parameters. The reported values are typical for raw municipal wastewater. Finally, it should be mentioned that the retentate, i.e. the reject water stream of the RO process, is diverted to the raw wastewater stream for treatment. This ensures that no wastewater is discharged to the environment and that a ZLD processes is carried out.

3.1.2 Calcined magnesite treated effluent

As shown in **Table 4**, calcined magnesite treatment has a high efficacy in the removal of both biological and particularly the nutrient content of raw wastewater. The pH of the raw wastewater was observed to be within the SANS 241-2: 2015 specifications. However, after treatment with calcined magnesite, it was observed that the pH of the effluent grossly increases. This is attributed to the addition of hydroxyl groups from the reaction of calcined magnesite with the raw wastewater. The reactions that govern the observed increase in the pH value of the treated effluent are shown in equation (1) and (2):

$$\mathrm{Mg/CaO} + \mathrm{H_2O} \rightarrow \mathrm{Mg/Ca(OH)_2} \quad (1)$$

$$\mathrm{Mg/Ca(OH)_2} \rightarrow \mathrm{Mg^{2+}/Ca^{2+}} + \mathrm{OH^-} \quad (2)$$

Furthermore, the high value of EC in the raw wastewater was observed to decrease after the treatment. This could be explained by the reaction of the calcined magnesite with the raw wastewater to form struvite. Specifically, struvite is sinking certain contaminants that are associated with the observed high EC value in the raw wastewater. Hence, their removal attenuates the EC value in the treated effluent, albeit the EC value is still above the drinking water limit. The same pattern was observed in the TDS value, which also decreased after treatment, but its level was still above the drinking water limit. Mn and Fe values were below

242 the SANS 241:2015-2 limits for drinking water in the raw wastewater, nonetheless calcined
243 magnesite treatment further reduced them to minuscule levels. Fe is a common inorganic
244 pollutant causing membrane fouling [31, 32], and hence its precipitation along with struvite is
245 beneficial for the membrane fouling inhibition. In addition, the results shown in Table 4,
246 indicate that the concentration of *E. coli*, total coliform, total plate counts, conductivity,
247 dissolved solids, and ammonia has been reduced but they are still above the SANS 241-
248 2:2015-2 limits. On the other hand, alkalinity, pH, Mg, Ca, colour and turbidity were
249 observed to increase after treatment. This may be attributed to the dissolution of Mg and Ca
250 from the matrices of calcined magnesite, hence leading to an increase in pH and alkalinity.
251 The existence of Mg and Ca was confirmed by FTIR, SEM-EDS and XRD techniques, as
252 reported below. This was expected since the thermally activated magnesite is rich in MgO,
253 while it also contains insignificant amounts of Ca. However, after RO treatment, high purity
254 potable water was obtained that meets the SANS 241-2:2015-2 specifications (Table 4).
255 Regarding the ammonia removal efficacy, this was observed to be dependent on phosphate
256 concentration, as the struvite formation is dependent on the molar ratio of the two. In this
257 work, approximately 87% and 98.8% removal efficacy for ammonia and phosphate
258 respectively, was observed. However, in this context one notable drawback is the system's
259 deficiency in phosphate, which is required to form a co-ordination of Mg, NH_3 and PO_4
260 reaction towards the synthesis of struvite, since a molar ratio of 1:1:1.1 is required. This
261 claim was also noted in a study by Tansel, et al. [33]. To this end, future research of our
262 group will focus on supplementing the phosphate level to enhance struvite synthesis. This
263 will also minimize the Mg concentration in the treated effluent, thus limiting the need of an
264 antiscalant.

265 Overall, it was found that calcined magnesite treatment can effectively remove ammonia and
266 phosphate, and possibly heavy metals such as zinc (Table 4), from municipal wastewater.
267 Attenuation of biological contaminants in the raw wastewater was also observed. This
268 suggests that this technology has some disinfection capabilities, which enable it to remove
269 biological contaminants. In a nutshell, struvite was successfully synthesized and the nutrient
270 load of the treated effluent was substantially attenuated. However, as was expected, the
271 chemical characteristics of the treatment effluent did not meet those for drinking water, as
272 specified in SANS 241-2:2015-2 (**Table 4**). Therefore, since in the context of this work
273 drinking water reclamation is also anticipated, the calcined magnesite treated effluent was
274 purified using RO and chlorination, as described below.

275 **3.1.3 Reverse osmosis purified water**

276 As shown in **Figure 1**, after the calcined magnesite treatment, the effluent was further
277 purified by a combination of chlorination and RO, as to reclaim drinking water. Specifically,
278 to disinfect the water and remove biological contamination first chlorine was added to the
279 calcined magnesite treated effluent. Hydrochloric acid was also added to drop the pH, as to
280 protect the RO membrane. This also contributed to the reduction of alkalinity (Table 4).
281 Then, the effluent was passed through the RO system. As shown in Table 4, the use of the
282 filtration technology efficiently reduced all examined parameters to meet the SANS 241-
283 2:2015-2 specifications for drinking water. Among others, the colour, turbidity, magnesium,
284 and calcium concentrations were drastically reduced. The RO treated water was then
285 chlorinated again, keeping the residual limit <5 mg L^{-1}, as to ensure that the water remains
286 disinfected throughout the supply chain until the end-user. Finally, the generated retentate is
287 sent back to the raw wastewater stream for treatment (**Figure 1**).

3.2 Struvite synthesis chemistry

It is well established that the removal of phosphate and ammonia from wastewater is mainly attributed to a combination of adsorption, crystallization, and precipitation. Adsorption precedes precipitation and then crystallization leads to the formation of struvite and the synthesis of other minerals [34]. Equation (3) and (4) show the possible routes for the formation of a number of product minerals during the treatment of municipal wastewater:

$$3Ca^{2+} + 2PO_4^{2-} = Ca_3(PO_4)_2 \quad (3)$$

$$Mg^{2+} + H_nPO_4^{n-3} + NH_4^+ + 6H_2O \rightarrow MgNH_4PO_4.6H_2O + nH^+ \quad (4)$$

where n = 0,1,2, etc., and it corresponds to the pH of the solution [35].

Furthermore, the presence of MgO and CaO within the matrices of the thermally activated cryptocrystalline magnesite will enable it to scavenge ammonia and phosphate via the crystallization of calcium, magnesium, phosphate and ammonia, as depicted in equations (3) – (6). This pattern was also reported by Peng, et al. [35]. Furthermore, this system cannot be purely defined by adsorption models, since the process is not reversible and it is not utterly a surface phenomenon. This suggests that it can be classified as a precipitation process with subsequent crystallization and it is within the branch of co-ordination chemistry. This allows the EC, TDS, and other contaminants to be reduced to acceptable limits.

3.3 Characterization of the raw and calcined cryptocrystalline magnesite and product minerals

According to the mass balance of this pilot unit approximately 52.5 kg of sludge per 3.5 m^3 will be produced. The product minerals contained in the produced sludge are also analyzed below, using different analytical techniques.

3.3.1 Mineralogical characterization

In **Figure 2,** the XRD patterns of the raw cryptocrystalline magnesite, the calcined magnesite, and the synthesized struvite are shown. Furthermore, Table 5 lists the identified mineral phases, along with the measured XRD peaks (2 theta degrees) and relevant studies that underpin the presented results.

Figure 2 here

Specifically, the identified 2 theta degrees of the raw cryptocrystalline magnesite (**Figure 2**) suggest that it is rich in magnesite, which is further corroborated by studies cited in Table 5. However, after calcination, new mineral phases, i.e. periclase and brucite, were observed in the calcined magnesite. This also indicates that CO_2 was released, as an airborne emission, from the matrices of cryptocrystalline magnesite, as shown in equation (5):

$$3MgCO_3 + Heat \rightarrow 3MgO + 3CO_2 \uparrow \quad (5)$$

Finally, the recovered struvite matrix was observed to contain, apart from struvite, quartz, brucite, periclase, and magnesite. These results not only confirm the synthesis of struvite through the proposed technology, but also the presence of other Mg-based minerals. The latter could be beneficial in cases where struvite is going to be used for agricultural soil amelioration and fertility enhancement.

Table 5 here

3.3.2 Metal functional groups

The metal functional groups of the raw cryptocrystalline magnesite, the calcined magnesite, and the synthesized struvite were identified using the FTIR technique. In **Figure 3** the FTIR

spectrum of raw and calcined magnesite and of the synthesized struvite are shown, while **Table 6** lists the identified metal functional groups, their wavenumber (cm^{-1}) and citations for relevant studies dealing with the identified metal functional groups.

Figure 3 here

As shown in **Figure 3** and **Table 6**, the metal functional groups of raw cryptocrystalline magnesite include carbonate and silicates, while water is also present. However, after calcination only the carbonates were still present and a new functional group of MgO was observed, which will be instrumental towards struvite crystallization. This confirms that CO_2 was volatilized and MgO was formed in the calcined magnesite matrix. The FTIR results also corroborate the ones obtained by the XRD technique. Furthermore, the presence of hydroxide (-OH) in both the calcined magnesite and the recovered struvite matrices suggest the possibility of brucite being present, which was confirmed in the XRD results. Regarding the recovered struvite, it was observed to contain PO_4^{3-}, N-H and MgO (**Table 6**), which confirms that indeed through the proposed technology struvite is formed. Hydroxide, along with carbonates were also observed. As mentioned above, hydroxide suggest the presence of brucite, while the carbonates could be attribute to the cryptocrystalline magnesite, as denoted by the XRD results. Finally, apart from suggesting that brucite might be present, prevalence of hydroxide also suggests that the synthesized struvite is hydrated, as shown in equation (6) [1]:

$$Mg^{2+} + NH_4^+ + PO_4^{3-} + 6H_2O \rightarrow MgNH_4PO_4.6H_2O \quad (6)$$

Table 6 here

3.3.3 Morphological characteristics

353 The morphology of the raw cryptocrystalline magnesite, the calcined magnesite, and the
354 synthesized struvite are shown in **Figure 4**. As mentioned in **Table 3** a high-resolution
355 Focused Ion Beam Scanning Electron Microscope (FIB FESEM) instrument was employed to
356 identify the morphological characteristics of the matrices under study. Specifically, an Auriga
357 Cobra FIB FESEM was used in this work, which can be also used for SEM imaging. Using
358 the FESEM function clear, ultra-high resolution, and low electrostatically distorted images
359 were obtained that revealed the morphology of the minerals under study (**Figure 4**).

360 ***Figure 4 here***

361 As shown in **Figure 4**, the raw cryptocrystalline magnesite has irregular sheets, which are
362 homogenously distributed across its surface. Furthermore, regardless of the different
363 magnification used, i.e. from 1μm to 100 nm, no changes in the morphological properties of
364 the raw cryptocrystalline magnesite surface were identified. The FESEM results also suggest
365 that cryptocrystalline magnesite is a nanomaterial with octagonal structures. However, after
366 calcination the morphology of the raw cryptocrystalline magnesite was observed to have
367 changed. This could be attributed to the fact that during calcination mass loss was observed,
368 attributed to CO_2 volatilization, which suggests that a reaction took place to form MgO. As a
369 result, after calcination the morphology of the calcined magnesite was observed to have
370 changed to round nanosheets, homogeneously distributed across its surface (**Figure 4**).
371 Finally, after the calcined magnesite comes into contact with the municipal effluent struvite is
372 synthetized, which was found to be rich in round nanosheets as well. Our group [1] and
373 various other groups have reported similar findings. For example, Heraldy, et al. [36]
374 reported that struvite can be present in different morphologies, such as coffin shaped,
375 pyramid type, prismatic type, needle type, and feather shaped, amongst others, and this is

strongly dependent on growth parameters and synthesis conditionsHeraldy, et al. [36]. Similar findings were reported by Chauhan and Joshi [37]. In addition, other Mg based minerals, apart from MgO, could have influenced the morphology of the synthesized struvite, along with impurities associated with the calcined magnesite matrix and micelles that would have been co-deposited with struvite during the synthesis process.

3.3.4 Spot analysis using HR-SEM

To further corroborate the elemental composition of the raw and calcined cryptocrystalline magnesite and of the synthesized struvite, spot-analysis, by means of Auriga Cobra FIB-FESEM instrument which includes an EDS detector, was employed. The morphological spot-analysis results of the raw cryptocrystalline magnesite, calcined magnesite, and synthesized struvite are shown in **Figure 5** to **Figure 7**, respectively.

Figure 5 here

As shown in **Figure 5a,** raw cryptocrystalline magnesite is predominated by octagonal structures on its surface. Elemental analysis further revealed that the predominant elements are C, Mg, and O, as well as traces (< 1%) of Ca and Si (**Figure 5b-f**). During the calcination process of the raw cryptocrystalline magnesite, C is the element that will be released in the environment through CO_2 volatilization. The EDS spot analysis results are also in agreement with the XRD and FTIR results for raw cryptocrystalline magnesite. Furthermore, the identified Ca and Si concentrations would be instrumental in increasing the pH of the raw wastewater effluent, if they would not be affected by the calcination process. Regarding the morphological properties of the calcined magnesite, these are shown in **Figure 6**.

Figure 6 here

Figure 6a portrays a nanosheet like morphology for the calcined cryptocrystalline magnesite. Furthermore, C, Mg, and O are the predominant elements in the calcined magnesite, while also traces of Ca, Si, Al, and Fe were observed. However, it should be noted that in spectrum no.156 a large Ca concentration (18.8%) was observed. These results are also in agreement with the XRD and FTIR results. Furthermore, it appears that the calcination process does not affect the Ca and Si levels that were observed in the raw cryptocrystalline magnesite matrix. These concentrations are pivotal for the chemical precipitation of nutrients from wastewater, since they will aid in increasing the pH of the raw wastewater. The pH increase will create the conditions that are suitable for the synthesis of struvite, since a defined alkaline pH range is required for struvite crystallization, as is well established in the literature [1, 15, 16, 38-40]. Finally, the morphological properties (SEM-EDS spot analysis) of the synthesized struvite are shown in **Figure 7**.

Figure 7 here

As shown in **Figure 7**, spherical and homogenous crystals were observed in the synthesized struvite. Furthermore, it was identified that the synthesized struvite is predominated by C, Mg, and O, while traces of Ca and Si were also observed. More importantly, the existence of P was identified, which confirms the synthesis of struvite. It should be noted that only the soluble component of calcined magnesite contributes to the synthesis of struvite and the non-soluble will settle. Moreover, the Mg and P content confirm struvite formation. Finally, the identified Si and Ca traces suggest the co-precipitation of struvite with those impurities. The obtained results are aligned with the ones obtained by the XRD and FTIR techniques.

3.3.5 Morphological features obtained by the HR-TEM analysis

The results regarding the morphological properties of raw cryptocrystalline magnesite, as well as the observed changes in the morphological properties of the calcined magnesite and the synthesized struvite are shown in **Figure 8**. In total, four different magnifications, i.e. 1μm, 500 nm, 200 nm, and a high-magnification of 100 nm, were used.

Specifically, as shown in **Figure 8** the raw cryptocrystalline magnesite has irregular nanosheets homogenously distributed across its surface, as was also identified in the FESEM analysis. Furthermore, regardless of the magnification the morphological properties of the raw cryptocrystalline magnesite were observed to remain the same. Moreover, **Figure 8** confirms that cryptocrystalline magnesite is a nanomaterial with octagonal to irregular structures. This corroborates, at least partially, the FESEM results. However, after calcination, the morphology of raw cryptocrystalline magnesite was observed to have changed. This could be attributed to the large CO_2 airborne emissions, during its calcination, to the atmosphere. More specifically, after calcination, the raw cryptocrystalline magnesite's morphology was observed to have changed to round nanosheets, (**Figure 8**). Furthermore, it was observed that the nanosheets are distributed homogeneously throughout the calcined magnesite's surface. Finally, after the calcined cryptocrystalline magnesite comes into contact with the raw municipal wastewater, this results to struvite synthesis. When using the four different magnifications, i.e. 1μm, 500 nm, 200 nm, and 100 nm, it is shown that the synthesized struvite is a nanomaterial with rich round nanosheets. This was also identified in the FESEM analysis.

Figure 8 here

3.4 Preliminary economic analysis of the struvite precipitation pilot unit

Overall, the results of this pilot study confirmed the feasibility, from the technical perspective, of struvite precipitation and recovery, as well as of drinking water reclamation from real municipal wastewater. However, the economic feasibility of the proposed technology remains largely unknown for the South African setting and thus was examined here through a preliminary cost-benefit analysis. The analysis includes the operational expenditure (OPEX) of the process, but not the capital expenditure (CAPEX) required for the construction of the pilot unit. The reason that the CAPEX was not included in the analysis is twofold. First and foremost, this study deals with a pilot unit and as such when the process is scaled up to more comprehensive systems, economies of scale would be achieved. Therefore, including the CAPEX of the pilot unit could skew the results and make them case specific. However, this is not the case for the OPEX, since the same amounts of chemical reagents would be consumed in scaled up systems, while a relative lower electricity input per unit of volume of wastewater might be required in scaled up system. However it was identified that the cost of electricity does not significantly affect the total cost of the process (Table 7). Second, this technology is versatile and could be even incorporated into existing wastewater treatment facility, thus largely avoiding CAPEX. Furthermore, it is a perquisite to treat the raw wastewater before being discharged to the environment, therefore its treatment will be associated with a cost regardless of the technology used. This suggest that a mean avoided cost would be required for conventional wastewater treatment, which could be ascribed to the system under study thus affecting the CAPEX of this technology. For the above reasons, CAPEX is not included in the economic analysis and a zero value was ascribed to the wastewater. Finally, the analysis was carried out in South African Rand (R) and then results were expressed using United States Dollar (USD). To provide context, the mean exchange rate of US dollar to rand was around R17 at the time of writing.

Table 7 here

Using the estimates shown in Table 7, a preliminary cost-benefit analysis, not including the CAPEX, was carried out for the 3.5 m^3 capacity pilot plant that is already constructed at the CSIR premises, in Pretoria, South Africa. By doing so, both the operating cost of treating municipal wastewater and the economic gains from the recovered struvite and the reclaimed drinking water were quantified and shown in **Table 7**. It was found that the OPEX to treat municipal wastewater treatment per run was calculated to be 0.8 USD per m^3 of wastewater. On the other hand, the economic gains from selling the generated products would amount to a maximum of 2.8 USD per m^3 of wastewater. It should be noted that the economic gains are just an estimate of the possible economic benefits of the process co-products, which does not include the cost of their further treatment, such as in the case of struvite, or their transportation cost. However, the results provide insight on the process economic sustainability and suggests that the process could be self-sustainable, from the economic perspective, providing a stable operating revenue to local communities. Furthermore, the results of this work appear to align with the literature, where this technology has been found economic viable, having a six year return of investment for larger plants with daily capacity in the range of few hundreds to few thousands m^3 [41].

4 Conclusions and recommendations

The findings from the 3.5 m^3 pilot plant that was examined in this work suggest that through a zero liquid discharge (ZLD) processes is feasible and economic viable to recover struvite and reclaim drinking water from municipal wastewater. The pilot plant under study was found to effectively treat real municipal wastewater and at the same time i) recover struvite (52.5 kg per run) and other mineral products, which can be particularly useful in the

agricultural industry, and ii) reclaim drinking water (3.4 m^3 per run), which meets the SANS 241:2015-2 specifications for drinking water. Future research will focus on the processing of struvite and of the Ca-based minerals towards the production of phosphoric acid.

Overall, this technology can provide the important water resource in water scarce regions and particularly in remote and insular communities in South Africa and further afield. This technology could be applied directly at village-level or further scaled up to industrial treatment systems. An additional stream of revenue will be also generated via the selling of the recovered struvite and the reclaimed drinking water. Specifically, through a preliminary economic analysis, the operational expenditure (OPEX) of the pilot unit was lower than the economic gains from the recovered struvite and the reclaimed water, suggesting that it can provide a stable operating revenue to local communities. Therefore, this technology can potentially be a game-changing approach in the endeavour to protect the environment and its precious resources at village-level in LMIC, where infrastructure is weak or non-existence, and possibly at more comprehensive scales for industrial wastewater treatment applications. Finally, future works of our group will focus on introducing cost effective alternatives to reverse osmosis (RO) filtration, such as the use of other more cost effective membrane filtration process, e.g. nanofiltration (NF) and ultrafiltration (UF) as well as on advanced oxidation processes (AOPs), e.g. photocatalysis, given the high number of annual sunshine hours in South Africa.

Acknowledgement

The authors of this manuscript would like to convey their sincere and profound gratitude to the Council for Scientific and Industrial research (CSIR), University of South Africa (UNISA), Magalies Water (MW), Tshwane University of Technology (TUT), Water

512 Research Commission (WRC), and the National Research Foundation (NRF) for extending
513 their facilities and funding towards the accomplishment of this project. Also, we would like
514 to thank the UK Global Challenges Research Fund for financial support.

References

[1] A. Mavhungu, R. Mbaya, V. Masindi, S. Foteinis, K.L. Muedi, I. Kortidis, E. Chatzisymeon, Wastewater treatment valorisation by simultaneously removing and recovering phosphate and ammonia from municipal effluents using a mechano-thermo activated magnesite technology, Journal of Environmental Management, 250 (2019) 109493.

[2] A.J. Ansari, F.I. Hai, W.E. Price, J.E. Drewes, L.D. Nghiem, Forward osmosis as a platform for resource recovery from municipal wastewater - A critical assessment of the literature, Journal of Membrane Science, 529 (2017) 195-206.

[3] J. Huang, N.R. Kankanamge, C. Chow, D.T. Welsh, T. Li, P.R. Teasdale, Removing ammonium from water and wastewater using cost-effective adsorbents: A review, Journal of Environmental Sciences, 63 (2018) 174-197.

[4] J.P. Vareda, A.J.M. Valente, L. Durães, Assessment of heavy metal pollution from anthropogenic activities and remediation strategies: A review, Journal of Environmental Management, 246 (2019) 101-118.

[5] O. Maaß, P. Grundmann, C. von Bock und Polach, Added-value from innovative value chains by establishing nutrient cycles via struvite, Resources, Conservation and Recycling, 87 (2014) 126-136.

[6] C. Gagnon, P. Turcotte, S. Trépanier, F. Gagné, P.J. Cejka, Impacts of municipal wastewater oxidative treatments: Changes in metal physical speciation and bioavailability, Chemosphere, 97 (2014) 86-91.

[7] A. Kunhikrishnan, N.S. Bolan, K. Müller, S. Laurenson, R. Naidu, W.-I. Kim, Chapter Five - The Influence of Wastewater Irrigation on the Transformation and Bioavailability of Heavy Metal(Loid)s in Soil, in: L.S. Donald (Ed.) Advances in Agronomy, Academic Press, 2012, pp. 215-297.

[8] J. De Waele, I.A. Nyambe, A. Di Gregorio, F. Di Gregorio, S. Simasiku, R. Follesa, S. Nkemba, Urban waste landfill planning and karstic groundwater resources in developing countries: the example of Lusaka (Zambia), Journal of African Earth Sciences, 39 (2004) 501-508.

[9] Q. Fu, B. Zheng, X. Zhao, L. Wang, C. Liu, Ammonia pollution characteristics of centralized drinking water sources in China, Journal of Environmental Sciences, 24 (2012) 1739-1743.

[10] G. Goshu, D. Byamukama, M. Manafi, A.K.T. Kirschner, A.H. Farnleitner, A pilot study on anthropogenic faecal pollution impact in Bahir Dar Gulf of Lake Tana, Northern Ethiopia, Ecohydrology & Hydrobiology, 10 (2010) 271-279.

[11] Z. Liu, K.M. Lompe, M. Mohseni, P.R. Bérubé, S. Sauvé, B. Barbeau, Biological ion exchange as an alternative to biological activated carbon for drinking water treatment, Water Research, 168 (2020) 115148.

[12] F. Ruiz-Beviá, M.J. Fernández-Torres, Effective catalytic removal of nitrates from drinking water: An unresolved problem?, Journal of Cleaner Production, 217 (2019) 398-408.

[13] Department of Water Affairs and Forestry, South African Water Quality Guidelines (first edition), Field Guide, Department of Water Affairs and Forestry, Volume 8 (1996).

[14] World Health Organization, Guidelines for drinking-water quality: fourth edition incorporating first addendum, 4th ed + 1st add ed., World Health Organization, Geneva, 2017.

[15] A.P. Bayuseno, W.W. Schmahl, Hydrothermal synthesis of struvite and its phase transition: Impacts of pH, heating and subsequent cooling methods, Journal of Crystal Growth, 498 (2018) 336-345.

[16] H. Wang, X. Wang, P. Xia, J. Song, R. Ma, H. Jing, Z. Zhang, X. Cheng, J. Zhao, Eco-friendly synthesis of self-existed magnesium oxide supported nanorod-like palygorskite for enhanced and simultaneous recovery of nutrients from simulated wastewater through adsorption and in-situ struvite formation, Applied Clay Science, 135 (2017) 418-426.

[17] S. Kataki, H. West, M. Clarke, D.C. Baruah, Phosphorus recovery as struvite from farm, municipal and industrial waste: Feedstock suitability, methods and pre-treatments, Waste Management, 49 (2016) 437-454.
[18] S. Sfez, S. De Meester, S.E. Vlaeminck, J. Dewulf, Improving the resource footprint evaluation of products recovered from wastewater: A discussion on appropriate allocation in the context of circular economy, Resources, Conservation and Recycling, 148 (2019) 132-144.
[19] D.o.E.a.S.A. The United Nations, The Sustainable Development Goals Report 2018, 2018.
[20] A. Mavhungu, S. Foteinis, R. Mbaya, V. Masindi, I. Kortidis, L. Mpenyana-Monyatsi, E. Chatzisymeon, Environmental sustainability of municipal wastewater treatment through struvite precipitation: Influence of operational parameters, Cleaner Production, Under review (2020).
[21] A.H. Ghabris, M. Abdel-Jawad, G.S. Aly, Municipal wastewater renovation by reverse osmosis state of the art, Desalination, 75 (1989) 213-240.
[22] S. Shanmuganathan, M.A.H. Johir, A. Listowski, S. Vigneswaran, J. Kandasamy, Sustainable Processes for Treatment of Waste Water Reverse Osmosis Concentrate to Achieve Zero Waste Discharge: A Detailed Study in Water Reclamation Plant, Procedia Environmental Sciences, 35 (2016) 930-937.
[23] M.F. Hamoda, N.F. Attia, I.A. Al-Ghusain, Performance evaluation of a wastewater reclamation plant using ultrafiltration and reverse osmosis, Desalination and Water Treatment, 54 (2015) 2928-2938.
[24] F. Tang, H.-Y. Hu, L.-J. Sun, Y.-X. Sun, N. Shi, J.C. Crittenden, Fouling characteristics of reverse osmosis membranes at different positions of a full-scale plant for municipal wastewater reclamation, Water Research, 90 (2016) 329-336.
[25] R. Kleemann, J. Chenoweth, R. Clift, S. Morse, P. Pearce, D. Saroj, Evaluation of local and national effects of recovering phosphorus at wastewater treatment plants: Lessons learned from the UK, Resources, Conservation and Recycling, 105 (2015) 347-359.
[26] P.M. Melia, A.B. Cundy, S.P. Sohi, P.S. Hooda, R. Busquets, Trends in the recovery of phosphorus in bioavailable forms from wastewater, Chemosphere, 186 (2017) 381-395.
[27] H. Huang, D. Xiao, Q. Zhang, L. Ding, Removal of ammonia from landfill leachate by struvite precipitation with the use of low-cost phosphate and magnesium sources, Journal of Environmental Management, 145 (2014) 191-198.
[28] S. Matta, K. Stephan, J. Stephan, R. Lteif, C. Goutaudier, J. Saab, Phosphoric acid production by attacking phosphate rock with recycled hexafluosilicic acid, International Journal of Mineral Processing, 161 (2017) 21-27.
[29] L. Egle, H. Rechberger, J. Krampe, M. Zessner, Phosphorus recovery from municipal wastewater: An integrated comparative technological, environmental and economic assessment of P recovery technologies, Science of the Total Environment, 571 (2016) 522-542.
[30] W. Ali, W.U. Rehman, M. Younas, M.I. Ahmad, S. Gul, Reverse osmosis as one-step wastewater treatment: a case study on groundwater pollution, 17 (2015) 42.
[31] F. Tang, H.Y. Hu, L.J. Sun, Y.X. Sun, N. Shi, J.C. Crittenden, Fouling characteristics of reverse osmosis membranes at different positions of a full-scale plant for municipal wastewater reclamation, Water Research, 90 (2016) 329-336.
[32] F. Tang, H.Y. Hu, L.J. Sun, Q.Y. Wu, Y.M. Jiang, Y.T. Guan, J.J. Huang, Fouling of reverse osmosis membrane for municipal wastewater reclamation: Autopsy results from a full-scale plant, Desalination, 349 (2014) 73-79.
[33] B. Tansel, G. Lunn, O. Monje, Struvite formation and decomposition characteristics for ammonia and phosphorus recovery: A review of magnesium-ammonia-phosphate interactions, Chemosphere, 194 (2018) 504-514.
[34] Z. Li, X. Sun, L. Huang, D. Liu, L. Yu, H. Wu, D. Wei, Phosphate adsorption and precipitation on calcite under calco-carbonic equilibrium condition, Chemosphere, 183 (2017) 419-428.

[35] L. Peng, H. Dai, Y. Wu, Y. Peng, X. Lu, A comprehensive review of phosphorus recovery from wastewater by crystallization processes, Chemosphere, 197 (2018) 768-781.
[36] E. Heraldy, F. Rahmawati, Heriyanto, D.P. Putra, Preparation of struvite from desalination waste, Journal of Environmental Chemical Engineering, 5 (2017) 1666-1675.
[37] C.K. Chauhan, M.J. Joshi, In vitro crystallization, characterization and growth-inhibition study of urinary type struvite crystals, Journal of Crystal Growth, 362 (2013) 330-337.
[38] E. Babaie, H. Zhou, B. Lin, S.B. Bhaduri, Influence of ethanol content in the precipitation medium on the composition, structure and reactivity of magnesium–calcium phosphate, Materials Science and Engineering: C, 53 (2015) 204-211.
[39] F. Mijangos, M. Kamel, G. Lesmes, D.N. Muraviev, Synthesis of struvite by ion exchange isothermal supersaturation technique, Reactive and Functional Polymers, 60 (2004) 151-161.
[40] P. Stolzenburg, A. Capdevielle, S. Teychené, B. Biscans, Struvite precipitation with MgO as a precursor: Application to wastewater treatment, Chemical Engineering Science, 133 (2015) 9-15.
[41] M.A. De Boer, A.G. Romeo-Hall, T.M. Rooimans, J.C. Slootweg, An Assessment of the Drivers and Barriers for the Deployment of Urban Phosphorus Recovery Technologies: A Case Study of The Netherlands, Sustainability, 10 (2018) 1790.
[42] V. Masindi, M.S. Osman, R. Shingwenyana, Valorization of acid mine drainage (AMD): A simplified approach to reclaim drinking water and synthesize valuable minerals – Pilot study, Journal of Environmental Chemical Engineering, 7 (2019) 103082.
[43] V. Masindi, J.G. Ndiritu, J.P. Maree, Fractional and step-wise recovery of chemical species from acid mine drainage using calcined cryptocrystalline magnesite nano-sheets: An experimental and geochemical modelling approach, Journal of Environmental Chemical Engineering, 6 (2018) 1634-1650.
[44] Y. Xu, Q. Zhong, X. Liu, Elemental mercury oxidation and adsorption on magnesite powder modified by Mn at low temperature, J. Haz. Mat, 283 (2015) 252-259.
[45] C.P. Eze, S.M. Nyale, R.O. Akinyeye, W.M. Gitari, S.A. Akinyemi, O.O. Fatoba, L.F. Petrik, Chemical, mineralogical and morphological changes in weathered coal fly ash: A case study of a brine impacted wet ash dump, Journal of Environmental Management, 129 (2013) 479-492.
[46] R. Li, J.J. Wang, B. Zhou, Z. Zhang, S. Liu, S. Lei, R. Xiao, Simultaneous capture removal of phosphate, ammonium and organic substances by MgO impregnated biochar and its potential use in swine wastewater treatment, Journal of Cleaner Production, 147 (2017) 96-107.
[47] X. Tang, L. Guo, C. Chen, Q. Liu, T. Li, Y. Zhu, The analysis of magnesium oxide hydration in three-phase reaction system, Journal of Solid State Chemistry, 213 (2014) 32-37.
[48] A.A. Rouff, Temperature-dependent phosphorus precipitation and chromium removal from struvite-saturated solutions, Journal of Colloid and Interface Science, 392 (2013) 343-348.
[49] J. Shu, H. Wu, M. Chen, H. Peng, B. Li, R. Liu, Z. Liu, B. Wang, T. Huang, Z. Hu, Fractional removal of manganese and ammonia nitrogen from electrolytic metal manganese residue leachate using carbonate and struvite precipitation, Water Research, 153 (2019) 229-238.
[50] J. Shu, H. Wu, M. Chen, L. Wei, B. Wang, B. Li, R. Liu, Z. Liu, Simultaneous optimizing removal of manganese and ammonia nitrogen from electrolytic metal manganese residue leachate using chemical equilibrium model, Ecotoxicology and Environmental Safety, 172 (2019) 273-280.
[51] H. Yan, K. Shih, Effects of calcium and ferric ions on struvite precipitation: A new assessment based on quantitative X-ray diffraction analysis, Water Research, 95 (2016) 310-318.
[52] F. Zeng, Q. Zhao, W. Jin, Y. Liu, K. Wang, D.-J. Lee, Struvite precipitation from anaerobic sludge supernatant and mixed fresh/stale human urine, Chemical Engineering Journal, 344 (2018) 254-261.
[53] W. Yin, H. Sun, J. Hong, S. Cao, B. Yang, C. Won, M. Song, Effect of Ca selective chelator BAPTA as depressant on flotation separation of magnesite from dolomite, Minerals Engineering, 144 (2019) 106050.

[54] N. Magagane, V. Masindi, M.M. Ramakokovhu, M.B. Shongwe, K.L. Muedi, Facile thermal activation of non-reactive cryptocrystalline magnesite and its application on the treatment of acid mine drainage, Journal of Environmental Management, 236 (2019) 499-509.
[55] A. Cahil, M. Najdoski, V. Stefov, Infrared and Raman spectra of magnesium ammonium phosphate hexahydrate (struvite) and its isomorphous analogues. IV. FTIR spectra of protiated and partially deuterated nickel ammonium phosphate hexahydrate and nickel potassium phosphate hexahydrate, Journal of Molecular Structure, 834-836 (2007) 408-413.
[56] L. Wei, T. Hong, X. Li, M. Li, Q. Zhang, T. Chen, New insights into the adsorption behavior and mechanism of alginic acid onto struvite crystals, Chemical Engineering Journal, 358 (2019) 1074-1082.

Tables' captions

Table 1: The five treatment stages for the synthesis of struvite and drinking water reclamation.

Table 2: The operating limits and membrane specification of the FilmTec™ RO membrane system [42].

Table 3: The equipment used to determine the parameters of the raw and the thermally activated magnesite and of the synthesized minerals (struvite).

Table 4: The chemical composition of wastewater and of the Mg and RO treated water, along with the South African National Standard (SANS) 241-2:2015 for drinking water.

Table 5: The measured XRD peaks (2 theta degrees) and the identified mineral phases of raw magnesite, calcined magnesite, and synthesized struvite, along with relevant studies for each mineral phase.

Table 6: The identified metal functional groups of the raw magnesite, calcined magnesite, and synthesized struvite.

Table 7: A preliminary cost-benefit analysis for the 3.5 m^3 pilot plant, in Pretoria, South Africa.

List of tables

Table 1: The five treatment stages for the synthesis of struvite and drinking water reclamation.

Number of stage	Unit process	Function
1	Struvite synthesis	To recover struvite
2	Holding tank	To store the treated water
3	Reverse osmosis (RO)	To purify the water
4	Storage tank	To store the purified water
5	Struvite storage tank	To store the dewatered struvite

Table 2: The operating limits and membrane specification of the FilmTec™ RO membrane system [42].

Parameter	**Values**
Product	BW30-4040
Part Number	80783
Surface Area m^2 (ft^2)	7.2 (78)
Feed Spacer Thickness (mil)	34
Permeate Flow Rate gpd (m^3/d)	2,400 (9.1)
Stabilized Salt Rejection (%)	99.5
Membrane Type	**Polyamide Thin-Film Composite**
Maximum Operating Temperature	45°C (113°F)
Maximum Operating Pressure	4.1 MPa (41 bar or 600 psi)
Feed Flow Rate: 4040	16 gpm (3.6 m^3/h)
Maximum Pressure Drop	15 psig (0.1 MPa or 1.0 bar)
Length in cm	101.6
Weight in kg	17.0
pH Range, Continuous Operation	2 - 11
pH Range, Short-Term Cleaning	1 - 13
Maximum Feed Silt Density Index	SDI 5
Free Chlorine Tolerance	<0.1 mg L^{-1}

Table 3: The equipment used to determine the parameters of the raw and the thermally activated magnesite and of the synthesized minerals (struvite).

Parameter	Equipment	Model
Mineralogical composition	XRD	PANalytical Aeris powder diffractometer with a PIXcel detector and fixed divergence- and receiving slits with Fe filtered Co-Kα radiation (λ=1.789Å). Phases were identified using X'Pert Highscore plus software.
Elemental composition	XRF	The Thermo Fisher ARL Perform'X Sequential XRF instrument with Uniquant software was used for analyses.
Morphology properties and spot-analysis	SEM-EDS	Auriga Cobra FIB-FESEM (Model: Sigma VP FE-SEM with Oxford EDS Sputtering System, Make: Carl Zeiss, Supplier: Carl Zeiss, USA)
Morphology properties	HR-TEM	High-Resolution Scanning Electron Microscope (HR- TEM) (JEM – 2100 electron microscope, Angus Crescent, Netherland)
Functional groups	FTIR	Perkin-Elmer Spectrum 100 Fourier Transform Infrared Spectrometer (FTIR) equipped with a Perkin-Elmer Precisely Universal Attenuated Total Reflectance (ATR) sampling accessory equipped with a diamond crystal

Table 4: The chemical composition of wastewater and of the Mg and RO treated water, along with the South African National Standard (SANS) 241-2:2015 for drinking water.

Analysis	Units	SANS 241:2015-2 Limits	Raw effluent	Mg treated	RO treated
E. coli	count/100mL	≤ 0	3,000	1,118	<0.001
Nitrate	mg L^{-1} N	≤ 10	1.5	<0.16	<0.16
Nitrite	mg L^{-1} N	≤ 0.90	0.20	<0.010	<0.010
Sulphate	mg L^{-1} SO_4^{2-}	≤ 500	50	13	<10
Total Chromium	µg L^{-1} Cr	≤ 50	70	<0.81	<0.5
Total Iron	µg L^{-1} Fe	≤ 2,000	67	54	<0.01
Total Manganese	µg L^{-1} Mn	≤ 400	50	<0.05	<0.01
Total Coliform	count per100mL	≤ 10	4,900	3,000	<0.001
Total Plate Count	count per1mL	≤ 1,000	570,000	24,000	<0.001
pH @ 25°C	-	≥ 5.00 to ≤ 9.70	7.76	10.25	7.5
Turbidity	NTU	≤ 1.00	3.32	5.37	<0.1
Colour	mg L^{-1} Pt-Co	≤ 15	31	33	<0.5
Electrical Conductivity	mS m^{-1}	≤ 170	327	211	20
Total Dissolved Solids	mg L^{-1}	≤ 1,200	1,458	1,062	258
Ammonia	mg L^{-1} NH_3	≤ 1.50	300	40	0.10
Total Sodium	mg L^{-1} Na	≤ 240	26	22	0.5
Total Zinc	mg L^{-1} Zn	≤ 5.0	<0.01	<0.01	<0.01
Temperature	ºC	≤ 30	25	26	25
Total Alkalinity	mg L^{-1} $CaCO_3$	≥ 250 to ≤ 300	138	350	<0.5
Total Calcium	mg L^{-1} Ca	≤ 300	16	19	0.9
Total Magnesium	mg L^{-1} Mg	≤ 100	15	278	0.5

Total Potassium	mg L^{-1} K	≤ 100	19	17	<1
Total Phosphate	mg L^{-1} P	≥ 1 to ≤ 10	180	2.19	<0.08

Table 5: The measured XRD peaks (2 theta degrees) and the identified mineral phases of raw magnesite, calcined magnesite, and synthesized struvite, along with relevant studies for each mineral phase.

Mineral	2 theta degree	Mineral phase	References
Raw magnesite	39	Magnesite	[1, 43, 44]
	41		
	42.5		
	50.5		
	52.5		
	60.5		
	62		
	72		
	73		
	79		
	81.5		
	82		
Calcined magnesite	21	Brucite	[16, 43, 45-47]
	42.5	Periclase	
	60	Brucite	
	69	Brucite	
	72	Periclase	
	81	Brucite	
Struvite	21	Brucite	[36, 38, 46, 48-52]

22	Struvite
31	Quartz
33	Calcite
39	Magnesite
44	Brucite
45	Struvite
50	Periclase/magnesite/struvite
60	Brucite
69	Quartz
72	Periclase
79	Struvite
82	Magnesite/Struvite

Table 6: The identified metal functional groups of the raw magnesite, calcined magnesite, and synthesized struvite.

Mineral	Wavenumber (cm^{-1})	Metal functional	References
Raw magnesite	750	CO_3 out-of-plane bending	[53, 54]
	905	vibration	
	1010		
	1050		
	1100		
	1200	Si-O-Si stretching	
	1400	CO_3	
	3000	H_2O	
Calcined magnesite	850	MgO	[1, 54]
	1400	CO_3	
	3700	-OH (Water)	
Struvite	850	MgO	[1, 16, 36, 50, 55, 56]
	1005	PO_4^{3-}	
	1200	PO_4^{3-}	
	1400	CO_3	
	1690	N-H	
	3000	-OH (Water)	
	3700	-OH (Water)	

Table 7: A preliminary cost-benefit analysis for the 3.5 m^3 pilot plant, in Pretoria, South Africa.

Raw materials and electricity	**Unit cost (USD)**	**Input**	Total cost (USD)/3.5 m^3
Wastewater	0	3500	0
Materials			
Calcined magnesite	205.8823529	0.0035	USD
Chlorine	235.2941176	0.00001	0.002353
HCl	705.8823529	0.00005	0.035294
Antiscalant	5294.117647	0.0001	0.529412
CIP chemicals	1058.823529	0.0001	0.105882
Total cost			**0.672941**
Electricity			
Wastewater feed pump	0.066470588	0.167	0.011101
Transfer pump	0.066470588	0.167	0.011101
RO feed pump	0.066470588	0.333	0.022135
Mixers	0.066470588	0.5	0.033235
Reagent mixers	0.066470588	0.25	0.016618
Reagent dosing	0.066470588	0.167	0.011101
RO dosing pumps	0.066470588	0.167	0.011101
RO membranes	0.066470588	0.167	0.011101
Total cost			**0.127491**
Overall cost			**0.800432**
Valuables			
Struvite	200	0.01	2
Clean water	0.535294118	3	1.605882
Total return			**3.605882**
Total commission for 3.5 KL			**2.805451**

The convention rate of 1 USD = 17 South African Rand on an average exchange rate.

Figures caption

Figure 1: The multi-stage treatment process for the synthesis of struvite and drinking water reclamation.

Figure 2: The X-ray diffractogram and mineralogical composition of raw magnesite, calcined magnesite and the synthesized struvite.

Figure 3: The metal functional groups of the raw magnesite, calcined magnesite, and synthesized struvite.

Figure 4: The FESEM images showing the changes in morphological properties of raw magnesite, calcined magnesite, and the synthesized struvite from lower to higher magnification, i.e. a) 1 μm, b) 200 nm, and c) 100 nm.

Figure 5: The SEM-EDS results of the raw magnesite showing (a) the spot analysis image and (b) to (f) the relevant EDS spectra.

Figure 6: The SEM-EDS results of the calcined raw magnesite showing (a) the spot analysis image and (b) to (f) the relevant EDS spectra.

Figure 7: The SEM-EDS results of the synthesized struvite showing (a) the spot analysis image and (b) to (f) the relevant EDS spectra.

Figure 8: The morphological properties of raw magnesite, calcined magnesite and the synthesized struvite using four magnifications, i.e. a) 1μm, b) 500 nm, c) 200 nm, and d) 100 nm.

List of figures

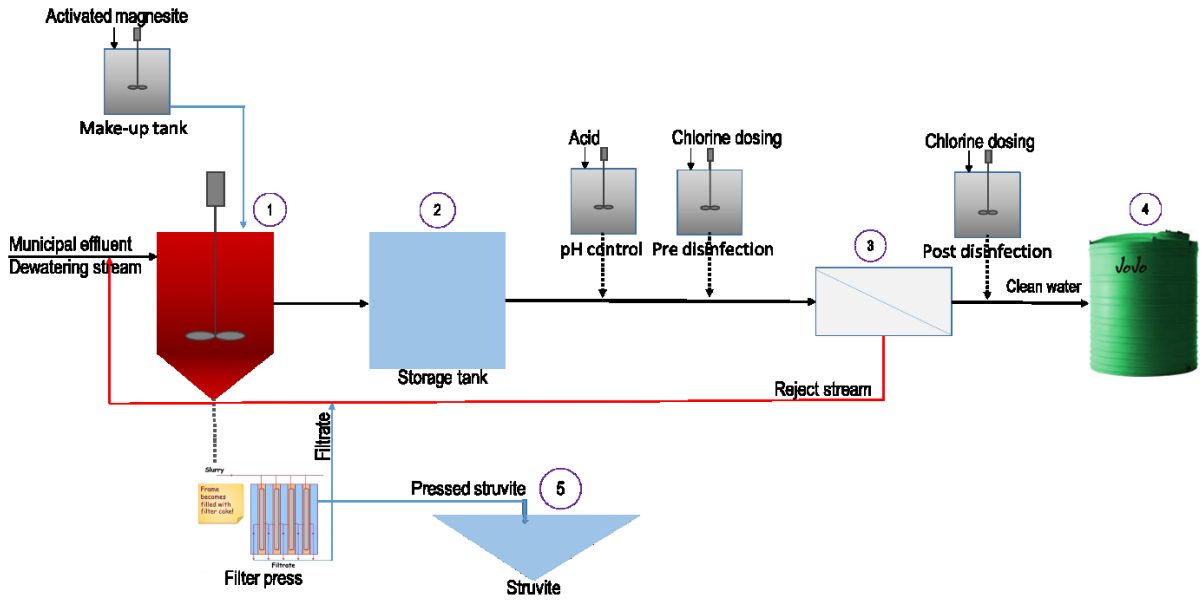

Figure 1: The multi-stage treatment process for the synthesis of struvite and drinking water reclamation.

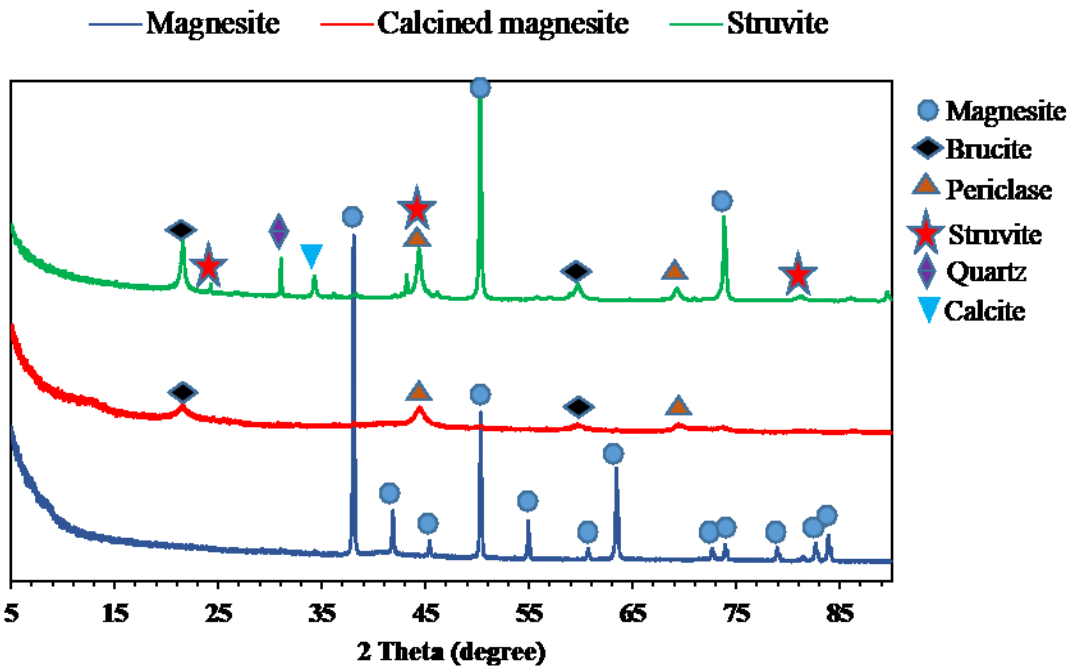

Figure 2: The X-ray diffractogram and mineralogical composition of raw magnesite, calcined magnesite and the synthesized struvite.

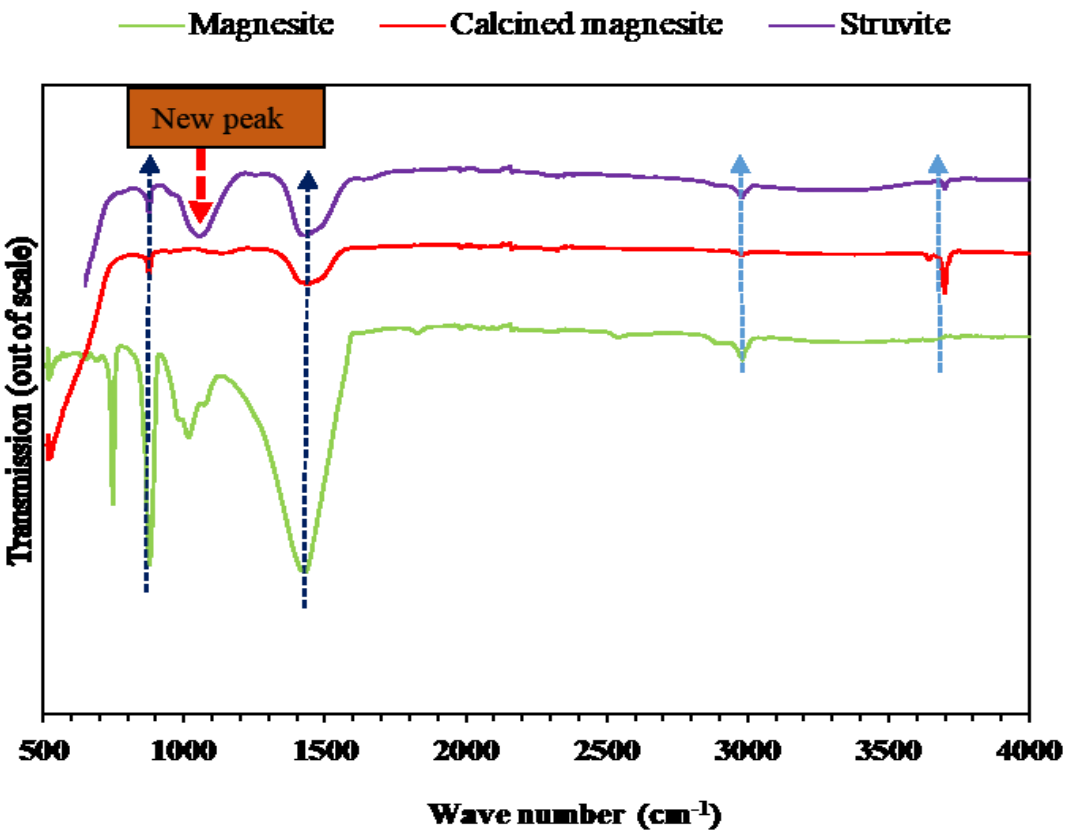

Figure 3: The metal functional groups of the raw magnesite, calcined magnesite, and synthesized struvite.

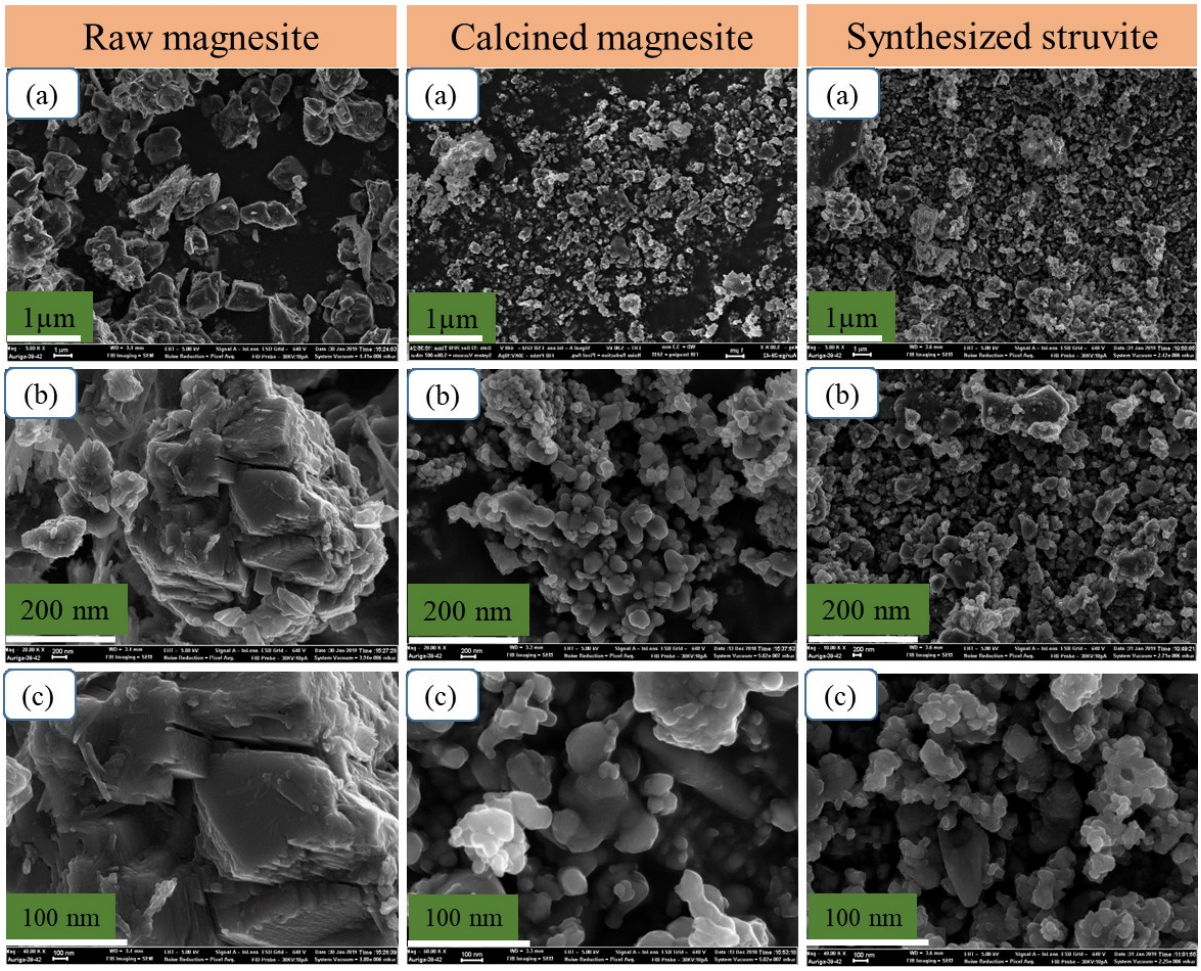

Figure 4: The FESEM images showing the changes in morphological properties of raw magnesite, calcined magnesite, and the synthesized struvite from lower to higher magnification, i.e. a) 1 µm, b) 200 nm, and c) 100 nm.

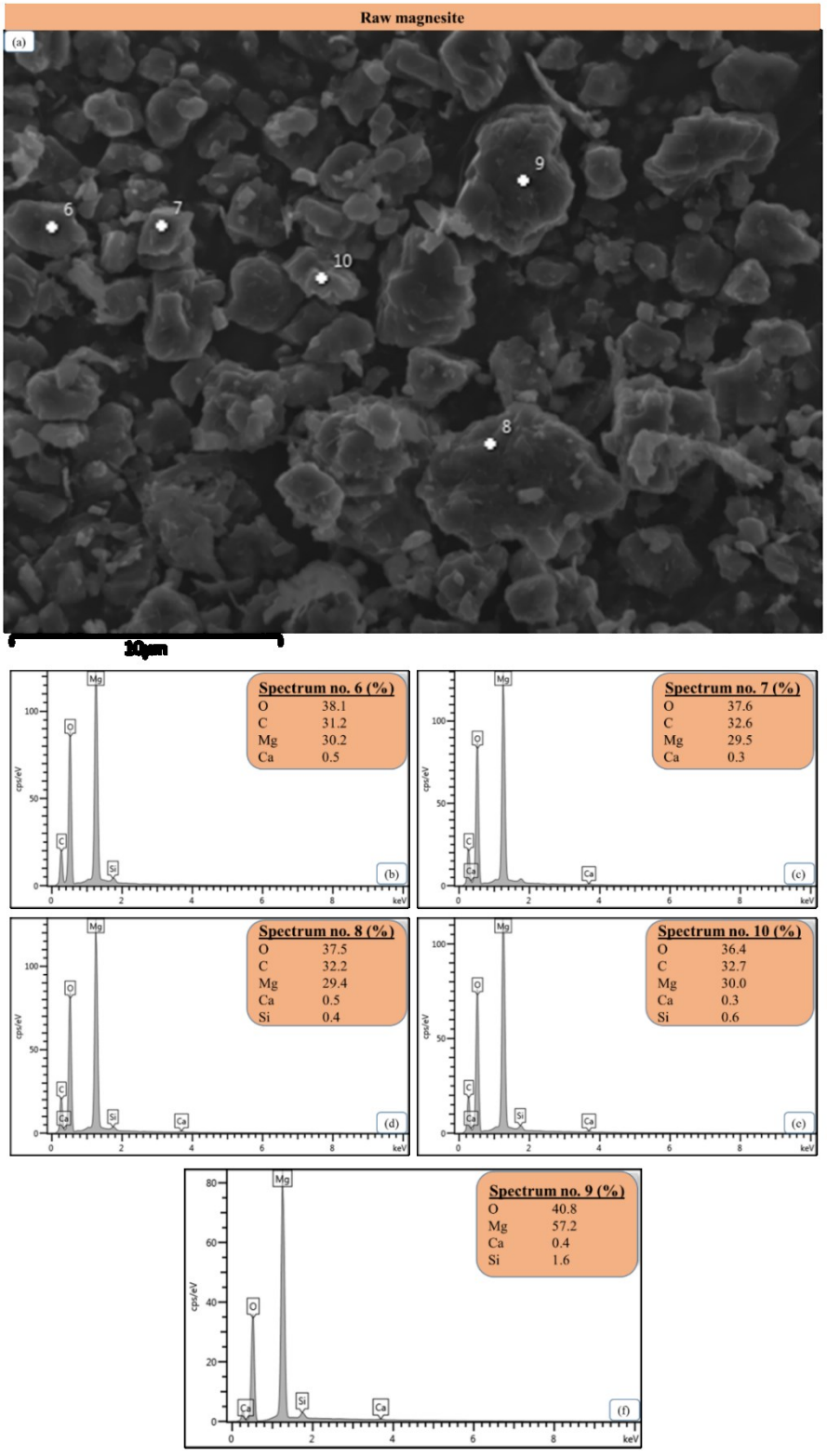

Figure 5: The SEM-EDS results of the raw magnesite showing (a) the spot analysis image and (b) to (f) the relevant EDS spectra.

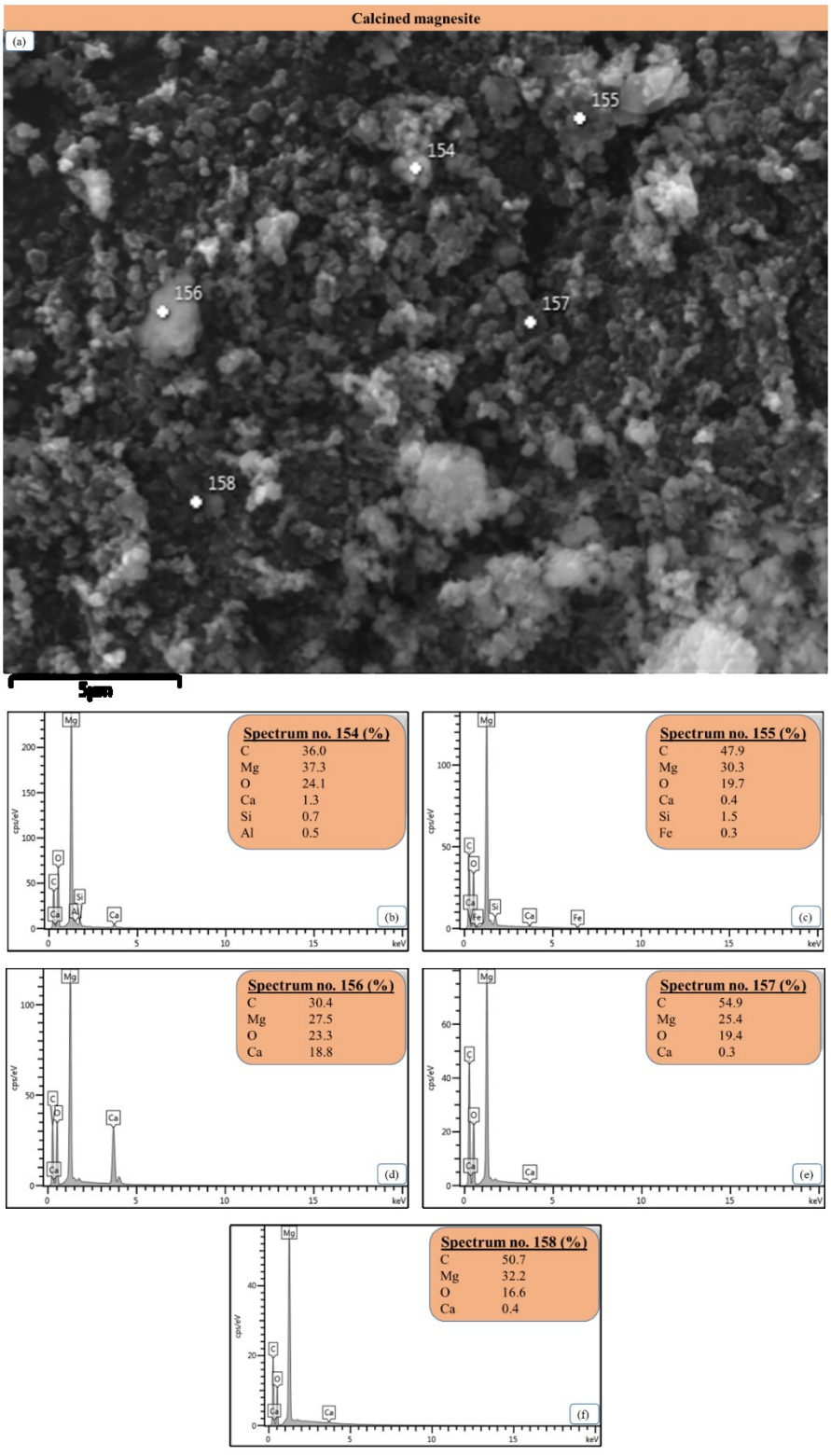

Figure 6: The SEM-EDS results of the calcined raw magnesite showing (a) the spot analysis image and (b) to (f) the relevant EDS spectra.

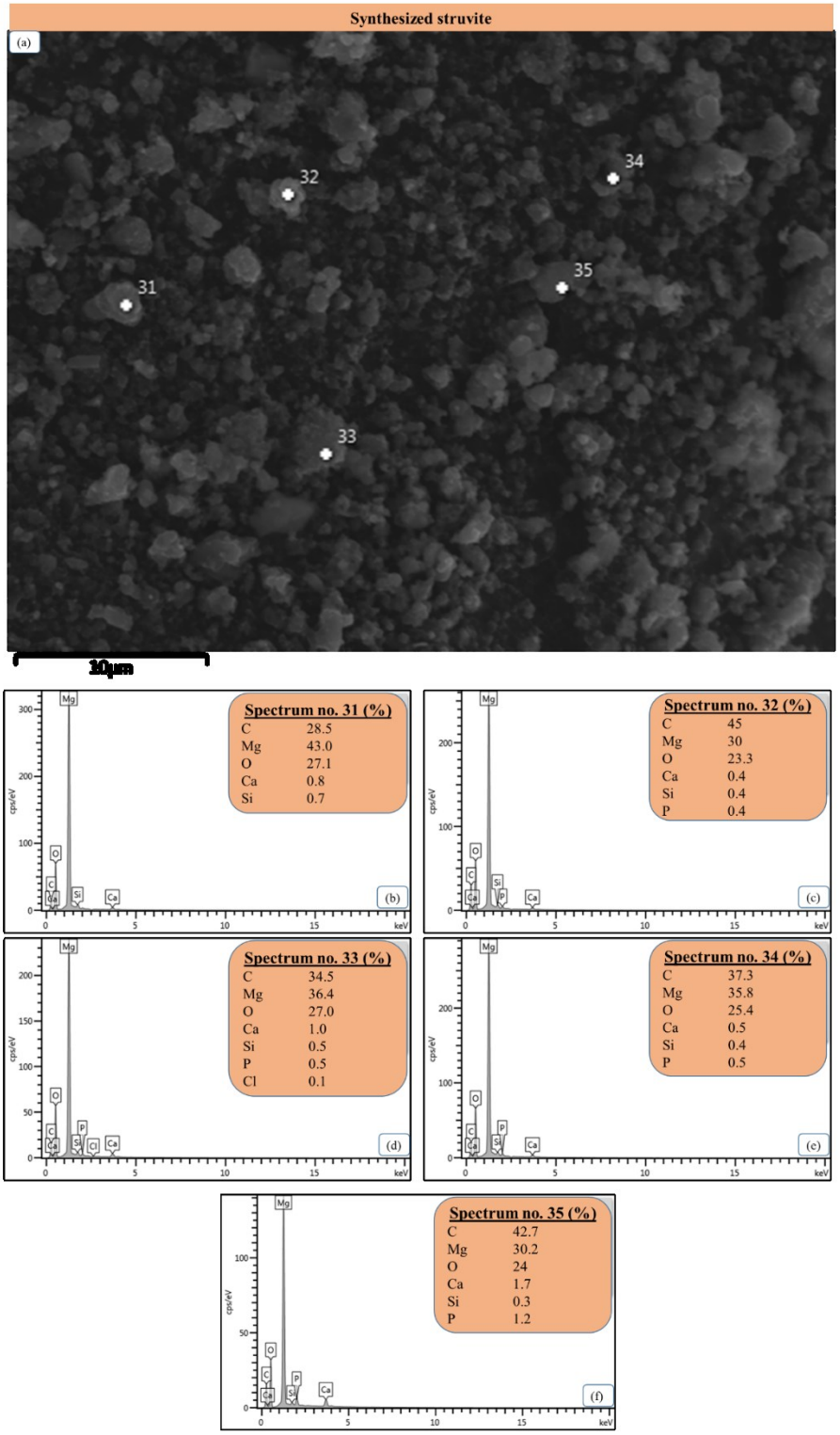

Figure 7: The SEM-EDS results of the synthesized struvite showing (a) the spot analysis image and (b) to (f) the relevant EDS spectra.

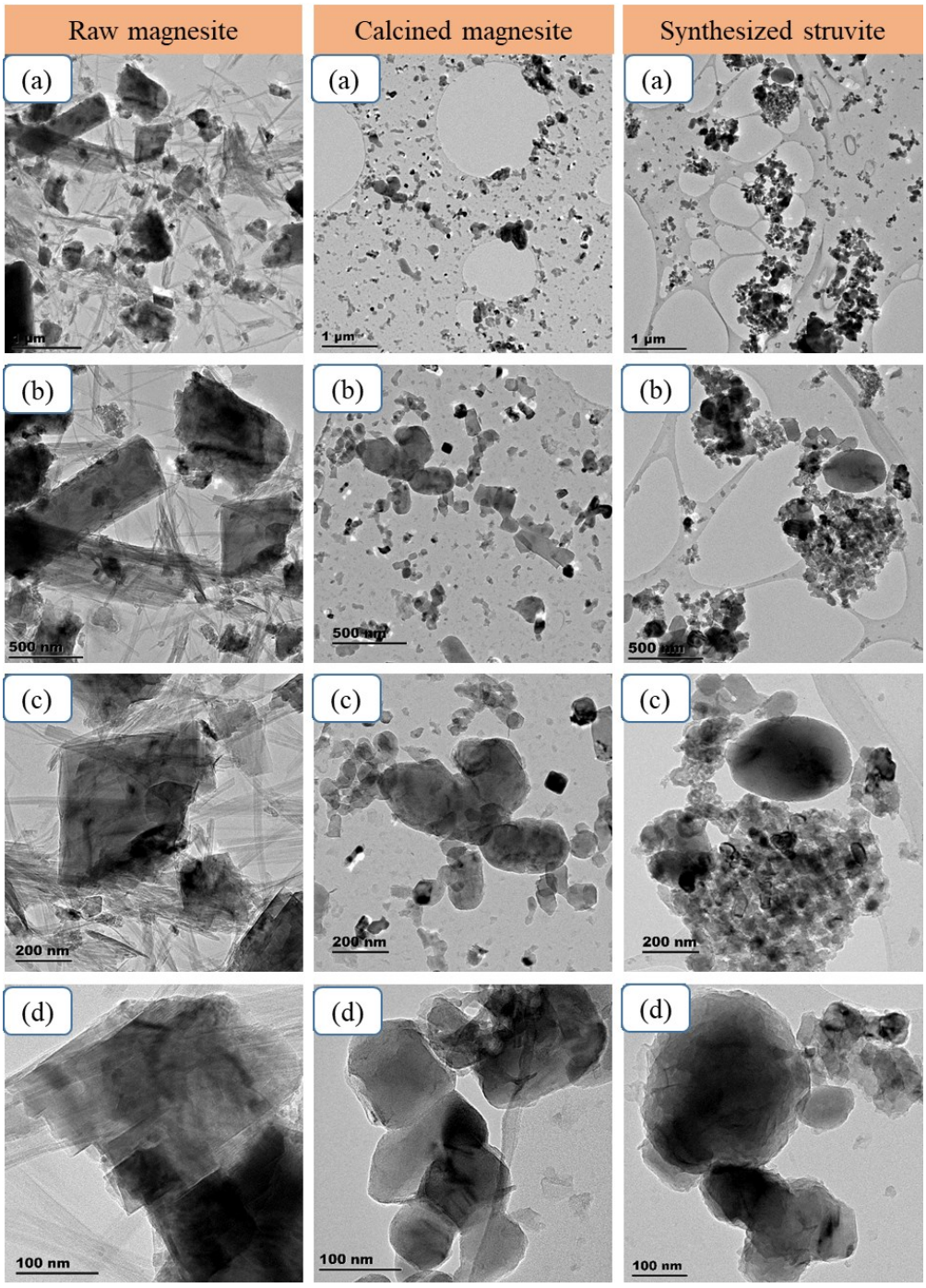

Figure 8: The morphological properties of raw magnesite, calcined magnesite and the synthesized struvite using four magnifications, i.e. a) 1µm, b) 500 nm, c) 200 nm, and d) 100 nm.